

Do stratocumulus clouds detrain? FIRE I data revisited

Stephan R. de Roode · Qing Wang

Received: 6 March 2006 / Accepted 4 July 2006 /
Published online: 19 October 2006
© Springer Science+Business Media B.V. 2006

Abstract Analyses of aircraft observations of the stratocumulus-topped boundary layer during the First ISCCP (International Satellite Cloud Climatology Project) Regional Experiment (FIRE I) show the frequent presence of clear, but relatively moist, air patches near the stratocumulus cloud-top interface. A conditional sampling of measurements in these clear air patches shows that their thermodynamic properties do more resemble boundary-layer air characteristics than those of free troposphere air. From an aircraft leg through cloud tops it is demonstrated that turbulent mixing across the cloud-top interface can lead to the local dissipation of the cloud top. Analogous to the terminology used for shallow cumulus parameterizations this process can be considered as detrainment, with which we mean that after a mixing event across the cloud-top boundaries, mixed unsaturated parcels become part of the clear environment of the cloud.

Keywords Aircraft observations · Boundary-layer clouds · Conditional sampling · FIRE I · ISCCP · Inversion structure · Stratocumulus

1 Introduction

The inversion layer capping the top of stratocumulus clouds can be very sharp. A tethered balloon sounding presented by Caughey and Kitchen (1984) shows a temperature jump of about 7 K over a vertical layer about 10 m thick. In stratocumulus clouds turbulence is generated by longwave radiative cooling at the cloud top and latent heat release effects in the cloud layer. Some turbulent eddies are able to penetrate into the

S. R. de Roode (✉)
Royal Netherlands Meteorological Institute (KNMI),
P.O. Box 201, 3730 AE, De Bilt, The Netherlands
e-mail: roode@knmi.nl

Q. Wang
Naval Postgraduate School, Monterey, CA, USA
e-mail: qwang@nps.edu

stable inversion, entrain pockets of inversion air, and mix them downward into the cloud layer. Because in this way relatively warm and dry inversion air is mixed into the stratocumulus cloud top, entrainment is one of the key processes controlling the evolution of the cloud layer (Nicholls and Turton 1986).

Deardorff et al. (1980) studied the entrainment zone of a convectively mixed-layer from laboratory experiments, and reported stringy regions of mixed-layer fluid that had become detached from the top of the mixed layer and sheared out. This detrained fluid remains visible for considerable periods of time because of reduced turbulent diffusion after being cut off from the rest of the mixed layer. Deardorff et al. also remarked that strong evidence of detrainment near the tops of stratocumulus clouds was reported earlier by Goodman and Miller (1976).

During the First ISCCP (International Satellite Cloud Climatology Project) Regional Experiment (FIRE I) holes and breaks in marine stratocumulus clouds were rather the rule than the exception (Paluch and Lenschow 1991). Siems et al. (1990) studied radiosonde soundings launched from San Nicolas Island during FIRE I, and concluded that the air above a stratocumulus cloud top is rarely homogeneous and often has haze layers, stable layers, or moist layers. They suggested that air above cloud top may have already been partly mixed with boundary-layer air.

Lenschow et al. (2000) analyzed horizontal aircraft legs through cloud tops from the Dynamics and Chemistry of Marine Stratocumulus (DYCOMS) experiment and noted that some boundary-layer air seems to leak across the cloud-top inversion and is mixed into the free atmosphere. Thus, some free atmosphere air may already have been modified by cloudy boundary-layer air. Recently, Gerber et al. (2005) proposed that detrainment of cloud causes conditioning of the entrainment interfacial layer with multiple mixing events until a buoyancy match is approached with cloud top. The fact that air just above the cloud top can be rather moist was also found from a large-eddy simulation (LES) study performed by Moeng et al. (2005).

Siems et al. (1990) hypothesized that wind-shear driven turbulence may lead to the local dissipation of the cloud top, but they were not able to verify this from the radiosonde observations used for their analysis. We will present aircraft observations collected during FIRE I to show that evaporation of cloud tops can result from turbulent mixing with relatively warm and dry air from just above the inversion layer. The observations also show the frequent presence of rather cold and moist clear air layers penetrating quite deeply into the cloud-topped boundary layer.

2 FIRE I observations

The FIRE I stratocumulus experiment took place during June and July 1987 off the coast of California (Betts and Boers 1990; Paluch and Lenschow 1991; Austin et al. 1995; Randall et al. 1996). We have selected four aircraft flights on the basis of the availability of horizontal legs in the boundary layer. Flight details and information about the atmospheric conditions are presented in Table 1. We use the following notation: SST denotes the sea surface temperature, BL top the boundary-layer top, FA base the base height of the free atmosphere, Δ the mean jump across the inversion layer located between the BL top and the FA base, $\theta_v = \theta(1 + 0.61q_v - q_l)$ the virtual potential temperature, θ is the potential temperature, q_v is the specific humidity, q_l is the liquid water content, $q_t = q_v + q_l$ is the total specific humidity, $\theta_l = \theta - \frac{L_v}{c_p} q_l$ is the liquid water potential temperature in its approximated form, L_v is the latent heat

Table 1 Summary of flight details

Flight	RF02B	RF03B	RF04B	RF08B
Date (1987)	30 June	02 July	05 July	14 July
Time [hh:mm:ss UTC]	20:53:21–23:53:20	02:58:02–05:58:01	19:52:38–22:52:37	19:26:46–22:26:45
Latitude	[30.0, 31.1]	[30.9, 31.8]	[31.6, 32.7]	[30.3, 31.5]
Longitude	[−122.6, −121.8]	[−122.6, −121.4]	[−122.1, −121.2]	[−124.1, −123.5]
SST [°C]	17.5	–	16.4	18.6
BL top [m]	887.5	837.5	787.5	787.5
FA base [m]	1087.5	1037.5	987.5	962.5
$\Delta\theta_v$ [K]	10.1	9.1	9.9	10.8
$\Delta\theta_l$ [K]	11.5	10.1	10.7	11.8
Δq_t [g kg ^{−1}]	−6.4	−4.9	−4.5	−4.3
max cloud fraction	1.0	1.0	0.9	1.0
max $q_{l,in-cloud}$ [g kg ^{−1}]	0.19	0.16	0.05	0.25
$u_{BL,top}$ [m s ^{−1}]	3.6	3.9	4.9	5.3
$v_{BL,top}$ [m s ^{−1}]	−2.2	−8.3	−10.6	−5.1
Δu [m s ^{−1}]	−1.2	1.8	−0.4	−1.2
Δv [m s ^{−1}]	2.8	5.7	5.6	−0.3
ΔO_3 [ppbv]	28.0	12.6	5.0	4.4
Ri_B	7.2	1.7	2.0	40.8

of vaporization of water, c_p is the constant pressure heat capacity of dry air, u and v are the east–west and north–south wind components, respectively, O_3 is the ozone concentration, and Ri_B is the bulk Richardson number across the mean inversion.

Figure 1 gives an example of the mean boundary-layer structure for Flight RF02B. Following the binning procedure of Rodts et al. (2003), the mean value for any arbitrary variable is computed from all aircraft data collected during one flight and within fixed height intervals with a depth $\Delta z = 25$ m. Thus, we used both horizontal as well as slant profiles. During each flight the aircraft flew ‘L’ or ‘V’ shaped patterns with linear transects of 50–100 km between approximate fixed positions. The mean values computed from the aircraft data may be loosely interpreted as typical grid-box mean values in a general circulation model and the standard deviation as a measure of subgrid variability.

The cloud fraction is computed from the Fast Forward-Scattering Spectrometer Probe (FSSP) measurements. To define a cloud point we used a threshold value well above the FSSP noise level, $q_{l,thres} = 0.01$ g kg^{−1}. Except for altitudes at about 800 m the mean cloud fraction is less than unity.

For height intervals within the boundary layer the standard variation gives a measure of mesoscale and turbulence generated fluctuations, in addition to temporal changes, and is relatively small. The boundary layer is characterized by vertically rather well-mixed profiles for quantities like the liquid water potential temperature θ_l , total water specific humidity q_t and ozone O_3 . The mean inversion layer is located between approximately 900 and 1100 m and is characterized by distinct vertical gradients. Note that cloud tops are present up to nearly 1000 m, which is well within the mean inversion zone. It should be noted that the binning procedure smears out local vertical gradients.

On the basis of the binned vertical profiles we diagnosed mean jumps across the inversion for different quantities. The top of the inversion layer was selected on the

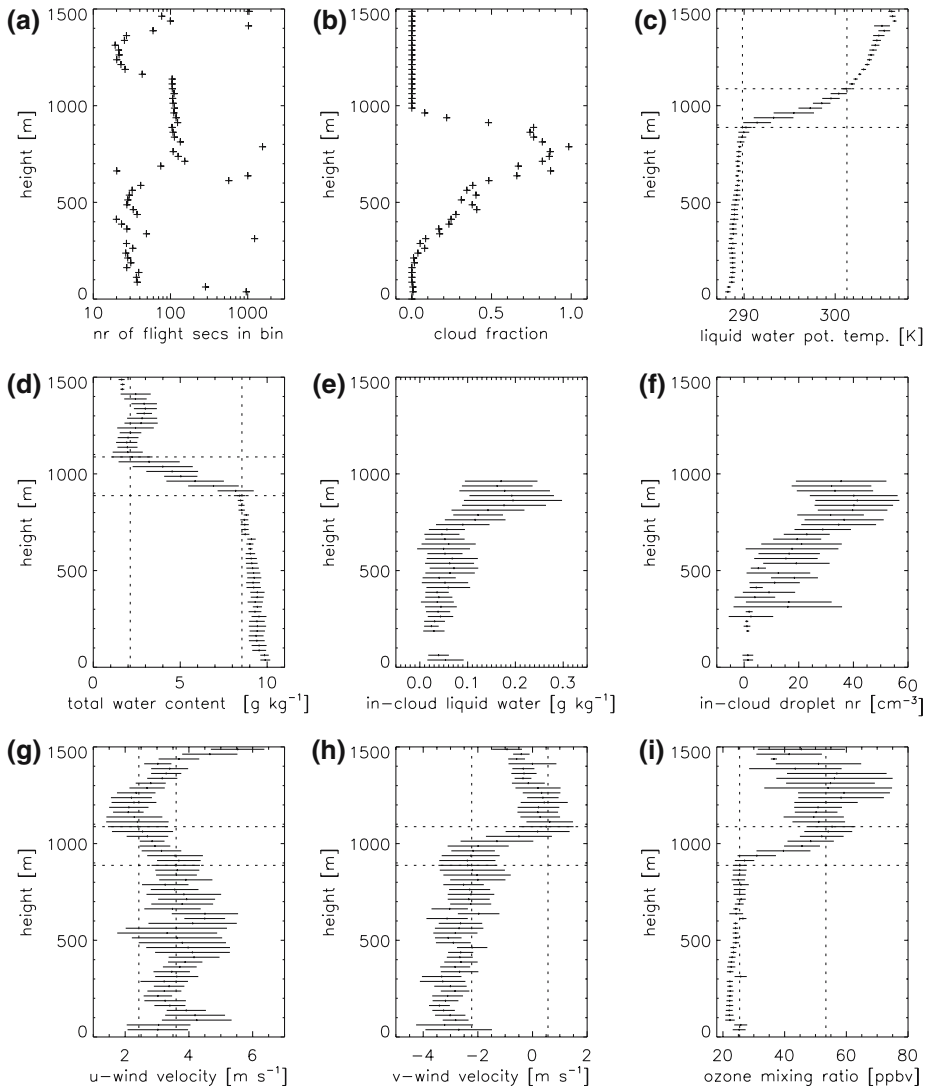


Fig. 1 Vertical profiles for **(a)** the number of flight seconds in each bin, **(b)** the cloud fraction, **(c)** the liquid water potential temperature (θ_l), **(d)** the total water content (q_t), **(e)** the in-cloud liquid water content (q_l), **(f)** the in-cloud droplet number concentration measured by the FSSP, **(g)** and **(h)** the horizontal east–west (u) and north–south (v) wind velocity components, respectively and **(i)** the ozone (O_3) mixing ratio during Flight RF02B. All mean values indicate bin-averaged values from all the data collected during the flight. In **(c)–(i)**, the error bars indicate one standard deviation from the bin-averaged mean values. The short-dashed horizontal lines indicate estimations of the mean heights of the boundary-layer top and the free atmosphere base. The vertical lines indicate the mean values of the quantities in the layer 100 m below the boundary-layer top and 100 m above the inversion top. Their values have been used to compute the mean inversion jumps

basis of vanishing vertical gradients of the total water content. For this quantity it can be seen that the mean jump is quite well defined, as q_t hardly varies with height just below and above the inversion. By contrast, diagnosing the top of the inversion at a higher altitude leads to a larger θ_l jump. Table 1 summarizes the heights of the mean

boundary-layer top and mean inversion layer depth for the FIRE I flights selected. Here the inversion jumps were computed from the bin-averaged vertical profiles.

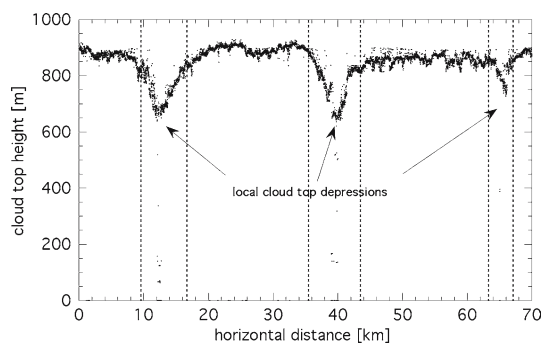
The binning procedure provides a good means of depicting the mean state of the atmosphere. However, local sharp inversion jumps just above cloud top will be smoothed out by the averaging procedure, in particular if the cloud-top height is variable in space. We will therefore investigate the local inversion structure from individual aircraft soundings through the cloud top.

3 Local inversion structure

Figure 2 shows three distinct depressions in the cloud-top height during Flight RF02B, and these local dips have a typical horizontal length scale on the order of a few kilometres. Likewise, measurements from flight legs within ≈ 150 m below cloud top collected during DYCOMS II showed tendrils of cloud free air between 200 and 800 m in width that possessed partial characteristics of free-tropospheric air (Faloona et al. 2005).

The lidar data were obtained in the same area in which a sequence of four slant aircraft soundings had been made just before. Two of these vertical profiles were flown either partly or entirely in clear-air areas. The clear air masses observed below the mean cloud-top height can therefore be regarded as being representative of the air above the local cloud top depressions. Using $q_{l,thres}$ as a threshold to distinguish between clear and cloudy air, we conditionally sampled the data from observations that were collected just prior to, and just after, the lidar run. Figure 3 shows that θ_l and q_l values in the clear air patches just above the local cloud-top depressions resemble more closely the values found in the boundary layer than in the free atmosphere. Note that the mean jumps diagnosed from the bin-average values during this flight were $\Delta\theta_l = 11.5$ K and $\Delta q_l = -6.4$ g kg $^{-1}$. Also the ozone observations indicate that the clear air masses below 900 m are predominantly originating from boundary-layer air. The in-cloud maximum value for the total water content just above 900 m is not a realistic value and represents a measurement error due to the wetting of the Lyman- α hygrometer sometimes found when the aircraft exited the cloud top. We did not encounter such erroneous spikes from descending soundings. We conclude that the bulk of this clear air mass consists of boundary-layer air remnants. Possible candidates explaining the local evaporation of cloud liquid water are heavy drizzle (Stevens et al. 2005), solar radiative heating, and entrainment.

Fig. 2 The cloud-top height determined from a lidar aboard the Electra aircraft during Flight RF02B. The leg was flown in a northerly direction along a longitude of about 122.6W between the latitudes 30.3 and 31.0N between 21:08:41 and 21:20:40 UTC



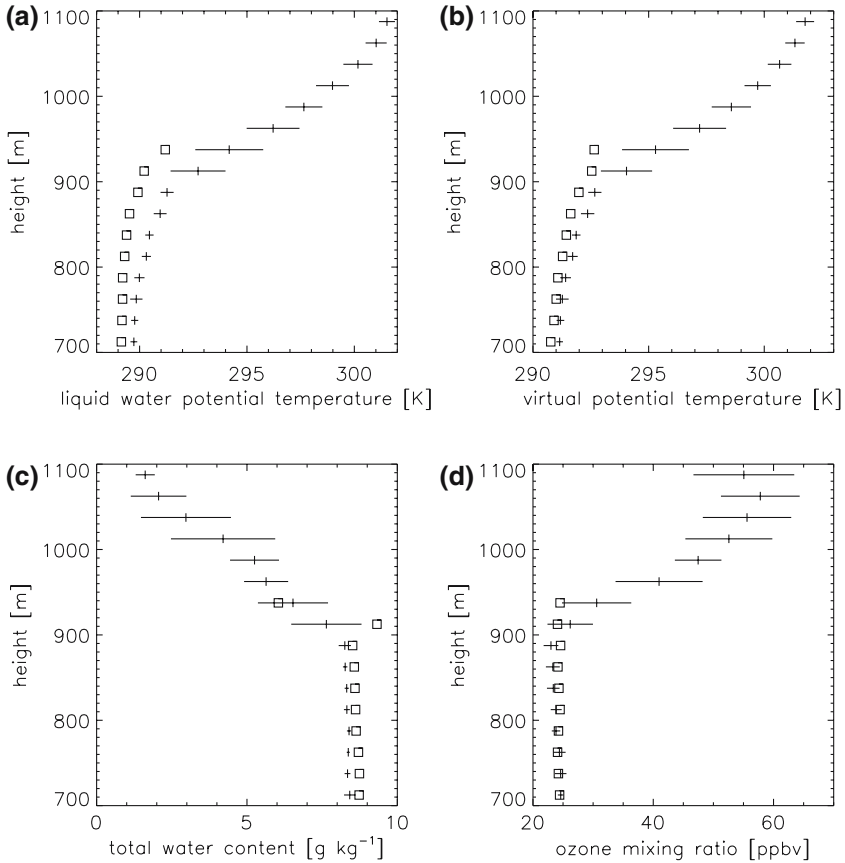


Fig. 3 Conditionally sampled mean in-cloud (open boxes ‘□’) and clear air values (plus symbols ‘+’, where the horizontal length indicates one standard deviation from the mean) from six aircraft slant profiles collected during Flight RF02B between 20:54:31 and 21:31:48 UTC. The standard deviation for the cloud points is not shown for the sake of visual clarity. Panel (a) shows the liquid water potential temperature, (b) the virtual potential temperature, (c) the total water content and (d) the ozone mixing ratio. For the height bin intervals between 700 and 900 m the minimum amount of total sampling time in one (clear) bin was 12 s, while the maximum total sampling time was 38 s in a (cloudy) bin

To obtain a more general appreciation of the mean thermodynamic structure of the clear air patches in the cloud layer Figs. 4 and 5 present conditionally sampled aircraft data during Flights RF04B and RF08B, respectively. Flight RF04B has a horizontally very inhomogeneous stratocumulus cloud layer with a rather low amount of cloud liquid water. By contrast, RF08B had much more cloud liquid water and between 600 and 800 m the cloud fraction is near unity. According to Paluch and Lenschow (1991) there is no precipitation reaching the surface during Flight RF04B, as opposed to Flight RF08B. Although both cases demonstrate that the clear-air patches below the mean cloud-top height have higher θ_t and lower q_t values, their large standard deviations suggest that the clear air masses are mixtures of free atmosphere and boundary-layer air. Lastly note that the cloud points exhibit a vertically well-mixed

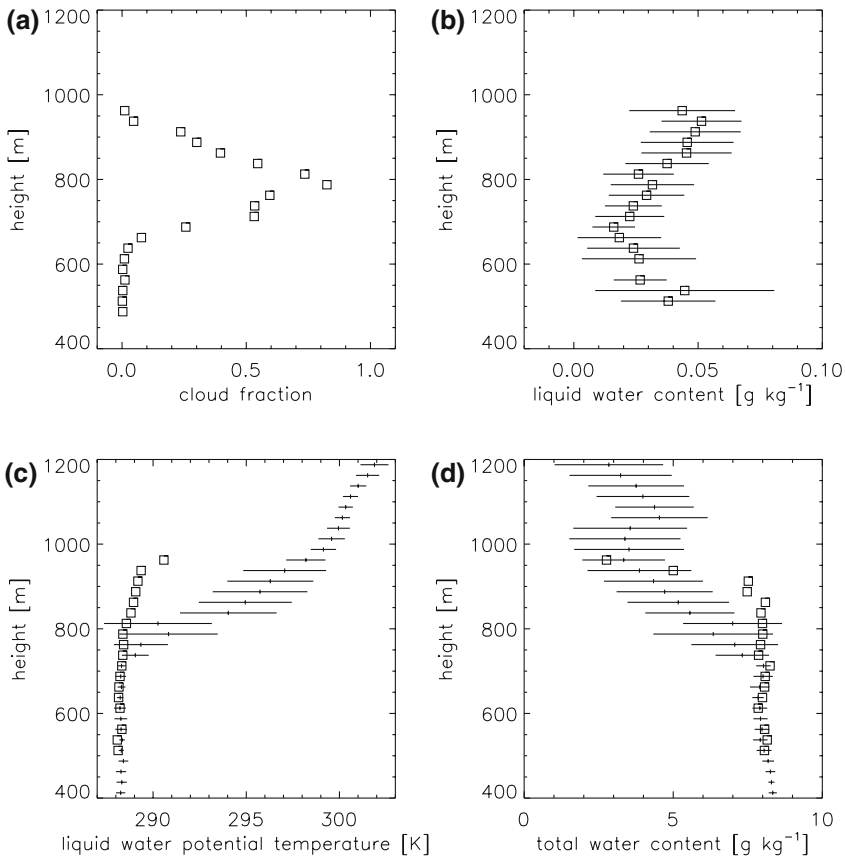


Fig. 4 Conditionally sampled mean values as a function of height from all aircraft data during run RF04B. Panel (a) shows the mean cloud fraction, (b) the mean and standard deviation of the liquid water content. Panel (c) shows the in-cloud (open boxes ‘□’) and clear air values (plus symbols ‘+’, with the length of the horizontal lines representing one standard deviation from the mean) for the liquid water potential temperature and (d) the total water content. The standard deviation for the cloud points is not shown for the sake of visual clarity

structure, which is likely due to vertical mixing induced by longwave radiative cooling near the cloud top.

Albrecht et al. (1985) observed that unsaturated regions in the transition zone near the inversion can have thermodynamic characteristics that are very close to the characteristics of the saturated air in the boundary layer and quite different from the characteristics of the unsaturated air above. Such a structure is clearly notable from Fig. 6, which displays observations from six subsequent sawtooth aircraft runs through the cloud-top region observed during Flight RF08B. It is remarkable that the clear air patches so closely resemble boundary-layer properties, having only a slightly larger liquid water potential temperature and smaller total water content in comparison to the mean jumps $\Delta\theta_l = 11.8$ K and $\Delta q_t = -4.3$ g kg⁻¹.

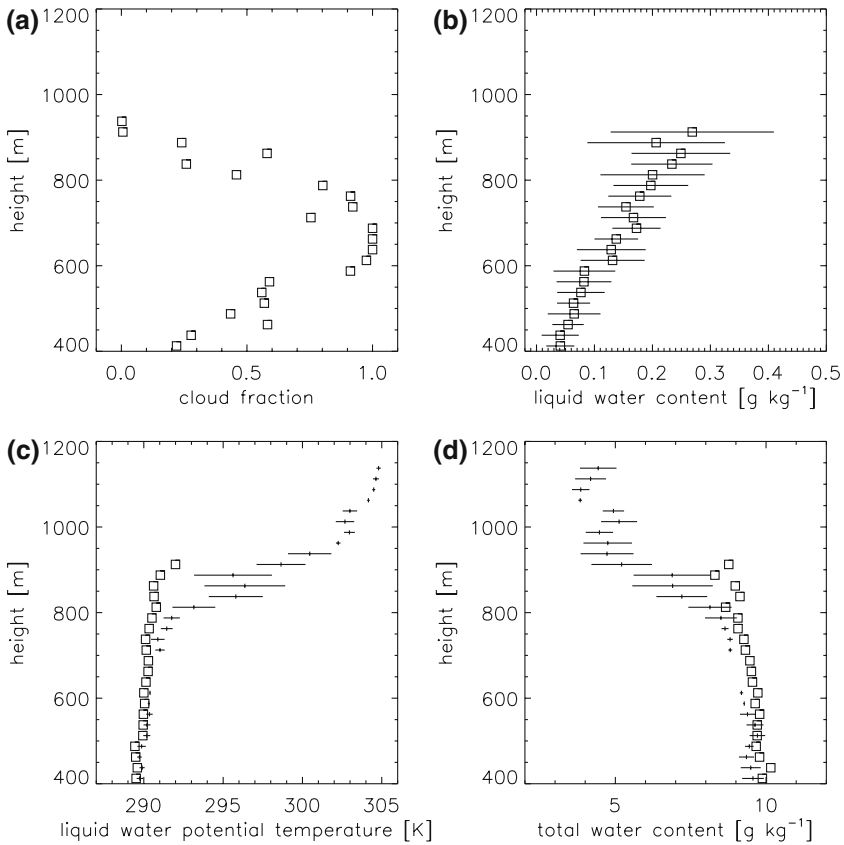


Fig. 5 As in Fig. 4, for RF08

4 Discussion: Can entrainment cause the local evaporation of cloud tops?

Albrecht et al. (1985) noted that if the air above the inversion is very dry and warm it has a large potential to evaporate cloud liquid water after mixing. This effect can be quantified from the critical mixing fraction χ_* , which defines the ratio of inversion air mass m_2 to the total mass of a mixed air parcel ($m_1 + m_2$) for which the mixture is just saturated, $\chi_* = \frac{m_1}{m_1 + m_2}$, with m_1 the mass of cloudy boundary layer-air. We computed χ_* for a maximum cloud liquid water content $q_{l,max} = 0.5 \text{ g kg}^{-1}$ at cloud top. Figure 7 shows χ_* as a function of the inversion jumps $\Delta\theta_1$ and Δq_t . Note that χ_* is proportional to the maximum liquid water content at the cloud top, and will therefore be smaller for smaller liquid water contents at cloud top (Stevens 2002). Clearly, the critical mixing fractions for the stratocumulus cloud decks observed during FIRE I are small and close to $\chi_* \sim 0.1$. Small values for χ_* imply that only a relatively small amount of air from just above the inversion is needed to evaporate a relatively large amount of cloud air. For example, a value $\chi_* = 0.1$ means that an air parcel from above the inversion has the potential to evaporate all the liquid water from a cloudy

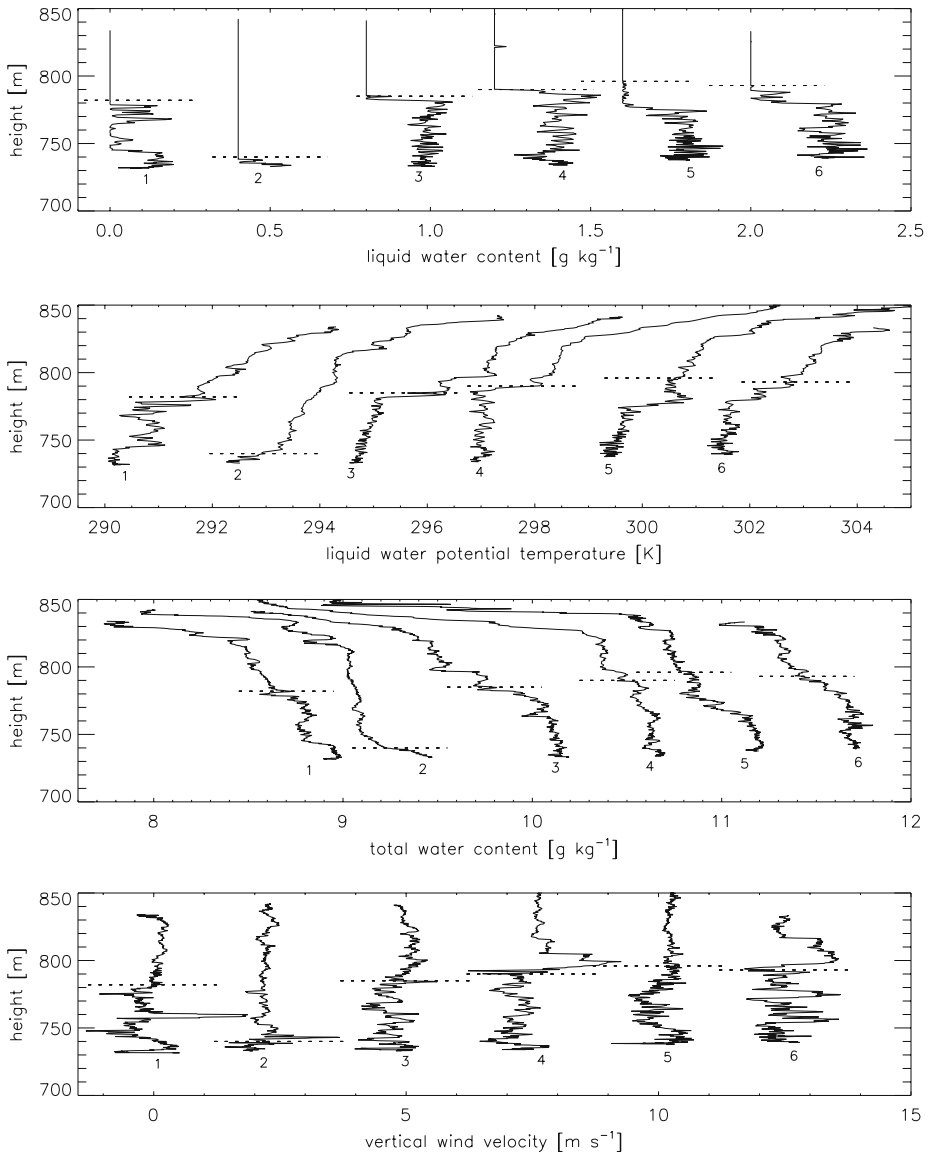


Fig. 6 Six quasi-vertical profiles observed from a continuous sawtooth flight pattern through the inversion region during Flight RF08B. To facilitate compact plotting, each vertical profile numbered N was shifted by a constant offset Δ_{off} with respect to profile $N-1$. **(a)** The liquid water content [0.4], **(b)** the liquid water potential temperature [2.3], **(c)** the total water content [0.5], and **(d)** the vertical velocity [2.5], where the value within the square brackets denotes Δ_{off} . The time interval of the observations was 2 min and 14 s

air parcel having nearly nine times the volume of the clear air parcel. If the mean inversion jumps are to the right of the buoyancy reversal criterion depicted by the $\Delta_2 = 0$ line in the figure, any mixed air parcel, either saturated or unsaturated, will be positively buoyant with respect to the cloud top (Randall 1980; Deardorff 1980).

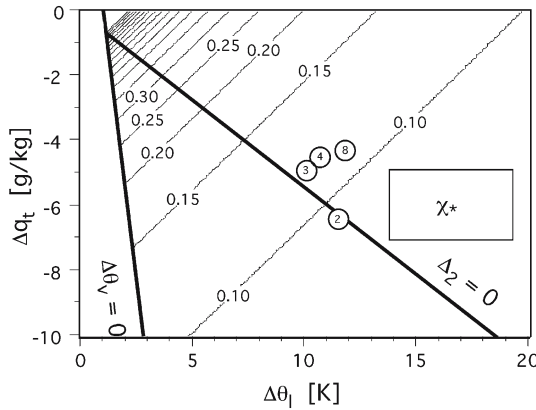


Fig. 7 The critical mixing fraction χ_* as a function of the inversion jumps $\Delta\theta_1$ and Δq_t . The numbered circles indicate the Flight numbers for the FIRE I stratocumulus cases considered, and their respective positions in the plot represent the inversion jumps according to Table 1. The thick line indicated by $\Delta v = 0$ represents the boundary of zero buoyancy jumps across the inversion for a clear boundary layer, whereas the $\Delta_2 = 0$ line indicates the buoyancy reversal criterion for the cloud-topped boundary layer

Figure 8 shows an example of cloud evaporation due to turbulent mixing during Flight RF03B. Some parts of this aircraft leg have the signature of clear free atmosphere air, with relatively large θ_1 and low q_t values and hardly any turbulence. The turbulent parts of the leg are distinguished by relatively large fluctuations in the three wind components. The vertically pointing arrows indicate areas with strongly anti-correlated q_t and θ_1 , and small or zero liquid water contents. The two arrows near 4 km show updrafts of about 200 m width, one has limited liquid water, one is clear. The clear updraft with boundary-layer air properties suggests local evaporation of the cloud droplets, likely to be caused by entrainment of clear air from just above the cloud interface. Similar results were also shown by Nicholls and Turton (1986) from aircraft observations in stratocumulus clouds over the North Sea.

The FIRE I aircraft observations seem to confirm the hypothesis of Siems et al. (1990) that cloud liquid water may be evaporated locally by wind-shear driven turbulence. Analogous to the terminology used for cumulus parameterizations this process may also be called detrainment, which means that after a mixing event across the cloud boundaries, unsaturated mixed parcels become part of the clear environment of the cloud, and vice versa for entrainment (Siebesma and Cuijpers 1995). In addition to shortwave radiative absorption and drizzle (VanZanten et al. 2005), evaporation caused by turbulent mixing may thus also play an important role in reducing the cloud liquid water amount.

On the basis of the aircraft observations we depict in Fig. 9 two possible scenarios following the entrainment of an air parcel from just above the inversion. Scenario I depicts the standard view of a free atmosphere air parcel that is entrained into cloud layer air, after which it is entirely diffused with cloud air. In this process there is sufficient turbulent kinetic energy available to be converted to potential energy needed for dragging down a positively buoyant clear air parcel and to subsequently mix it with cloud air.

The second scenario hypothesizes that the bulk of the turbulent kinetic energy has been consumed by the entrainment process leaving insufficient turbulent kinetic

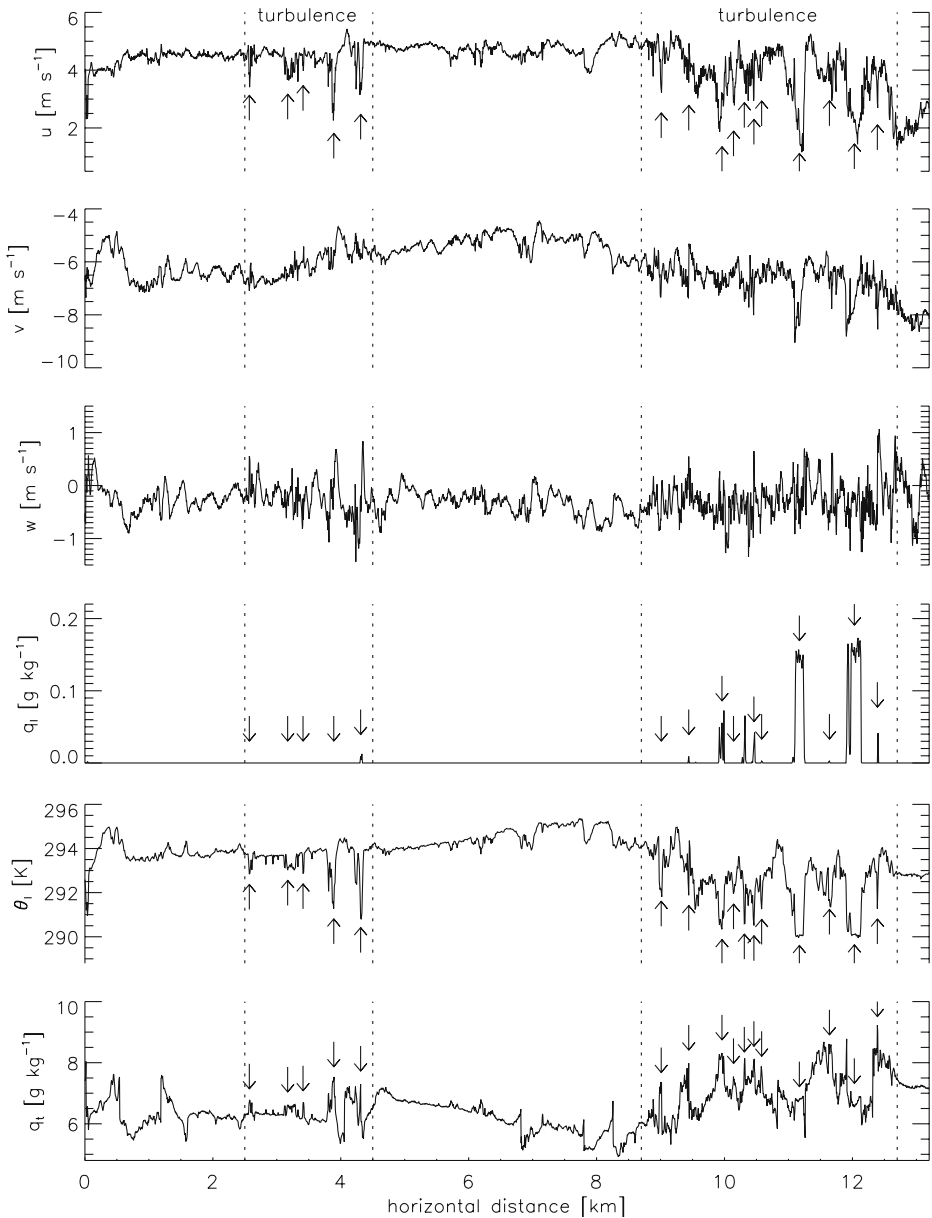
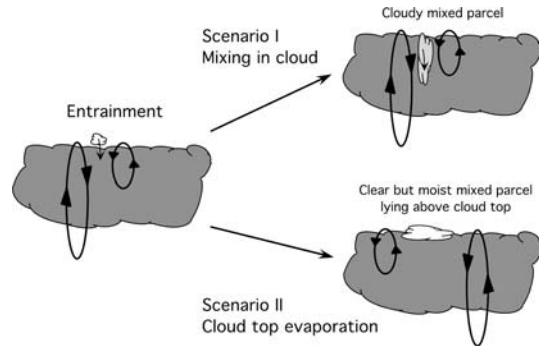


Fig. 8 Observations from a horizontal run during Flight RF03B for the east–west (u), north–south (v) and vertical wind (w) velocities, respectively, the liquid water content (q_l), the liquid water potential temperature (θ_l) and the total water content (q_t), at an altitude of 870 m

energy for full mixing resulting in a partly mixed, moist, but clear layer overlying the cloud top. Because this layer is detached from the turbulent cloud layer it may persist to lie above the local cloud-top interface on relatively long time scales (Dear-dorff et al. 1980). The formation of such a layer changes the local jump conditions across the cloud top. Because the intensity of mixing across the cloud-top interface

Fig. 9 Two possible scenarios following entrainment and subsequent mixing of an air parcel from just above the inversion with cloud layer air. In Scenario I the mixed parcel contains liquid water and is entirely diffused into the cloudy boundary layer. In Scenario II the mixed parcel is moist but clear and rests on top of the cloud layer whose top has been lowered locally due to evaporation of cloud liquid water



depends critically on the inversion jump structure, the results presented here lead to the question: what role do these layers play in the temporal evolution and lifetime of a stratocumulus cloud layer?

Acknowledgements Stephan de Roode did part of this work as a visiting scientist at the Naval Postgraduate School in Monterey, California, and is happy to thank NPS for its hospitality and for financially supporting his stay. Qing Wang's Work and Stephan de Roode's NPS visit was supported by the office of Naval Research Award N0001403 WR20193. Qing wang was also supported by NSF Grant ATM – 9900496. Part of this research project was carried out in the framework the Dutch National Research Programme Climate changes Spatial Planning (www.klimaatvoorruijnte.nl). The FIRE I aircraft data were gratefully obtained from the NASA Langley Research Center Atmospheric Sciences Data Center. We thank Margreet van Zanten for critically reading the manuscript and Harm Jonker for useful discussions on his observations of detrainment in the convection tank of Delft Technical University.

References

- Albrecht BA, Penc RS, Schubert WH (1985) An observational study of cloud-topped mixed-layers. *J Atmos Sci* 42:800–822
- Austin P, Wang Y, Kujala V, Pincus R (1995) Precipitation in stratocumulus clouds: Observational and modeling results. *J Atmos Sci* 52:2329–2352
- Betts AK, Boers R (1990) A cloudiness transition in a marine boundary layer. *J Atmos Sci* 47:1480–1497
- Caughey SJ, Kitchen M (1984) Simultaneous measurements of the turbulent and microphysical structure of nocturnal stratocumulus cloud. *Quart J Roy Meteorol Soc* 110:13–34
- Deardorff JW, Willis GE, Stockton BH (1980) Laboratory studies of the entrainment zone of a convectively mixed layer. *J Fluid Mech* 100:41–64
- Deardorff JW (1980) Cloud-top entrainment instability. *J Atmos Sci* 37:131–147
- Faloona I, Lenschow DH, Campos T, Stevens B, Van Zanten MV, Blomquist B, Thornton D, Bandy A, Gerber H (2005) Observations of entrainment in eastern Pacific Marine stratocumulus using three conserved scalars. *J Atmos Sci* 62:3268–3285
- Gerber H, Frick G, Malinowski SP, Brenguier SL, Burnet F (2005) Holes and entrainment in stratocumulus. *J Atmos Sci* 62:443–459
- Goodman JK, Miller A (1976) Mass transport across a temperature inversion. Technical Report 76-10, San Jose State University, Dept. of Meteorology
- Lenschow DH, Zhou MY, Zeng XB, Chen LS, Xu XD (2000) Measurements of fine-scale structure at the top of marine stratocumulus. *Boundary-Layer Meteorol* 97:331–357
- Moeng CH, Stevens B, Sullivan PP (2005) Where is the interface of the stratocumulus-topped PBL? *J Atmos Sci* 62:2626–2631
- Nicholls S, Turton JD (1986) An observational study of the structure of stratiform cloud sheets: Part II. Entrainment. *Quart J Roy Meteorol Soc* 112:461–480

- Paluch IR, Lenschow DH (1991) Stratiform cloud formation in the marine boundary layer. *J Atmos Sci* 48:2141–2158
- Randall DA, Albrecht BA, Cox SK, Johnson D, Minnis P, Rossow W, Starr DO (1996) On FIRE at ten. *Adv Geophys* 38:37–177
- Randall DA (1980) Conditional instability of the first kind upside down. *J Atmos Sci* 37:125–130
- Rodts SMA, Duynkerke PG, Jonker HJJ (2003) Size distributions and dynamical properties of shallow cumulus clouds from aircraft observations and satellite data. *J Atmos Sci* 60:1895–1912
- Siebesma AP, Cuijpers JWM (1995) Evaluation of parametric assumptions for shallow cumulus convection. *J Atmos Sci* 52:650–666
- Siems ST, Bretherton CS, Baker MB, Shy S, Breidenthal RE (1990) Buoyancy reversal and cloud-top entrainment instability. *Quart J Roy Meteorol Soc* 116:705–739
- Stevens B, Vali G, Comstock K, Wood R, van Zanten MC, Austin PH, Bretherton CS, Lenschow DH (2005) Pockets of open cells (POCs) and drizzle in marine stratocumulus. *Bull Amer Meteorol Soc* 86:51–57
- Stevens B (2002) Entrainment in stratocumulus-topped mixed layers. *Quart J Roy Meteorol Soc* 128:2663–2690
- VanZanten MC, Stevens B, Vali G, Lenschow DH (2005) Observations of drizzle in nocturnal marine stratocumulus. *J Atmos Sci* 62:88–106